Approximate quasiparticle correction for calculations of the energy gap in two-dimensional materials

I. Guilhon,[1,*] D. S. Koda,[1,†] L. G. Ferreira,[2] M. Marques,[1,‡] and L. K. Teles[1,§]

[1]*Grupo de Materiais Semicondutores e Nanotecnologia, Instituto Tecnológico de Aeronáutica, DCTA, 12228-900 São José dos Campos, Brazil*

[2]*Instituto de Física, Universidade de São Paulo, CP 66318, 05315-970 São Paulo, SP, Brazil*

(Received 29 November 2017; published 24 January 2018)

At the same time that two-dimensional (2D) systems open possibilities for new physics and applications, they present a higher challenge for electronic structure calculations, especially concerning excitations. The achievement of a fast and accurate practical model that incorporates approximate quasiparticle corrections can further open an avenue for more reliable band structure calculations of complex systems such as interactions of 2D materials with substrates or molecules, as well as the formation of van der Waals heterostructures. In this work, we demonstrate that the performance of the fast and parameter-free DFT-1/2 method is comparable with state-of-the-art *GW* and superior to the HSE06 hybrid functional in the majority set of the 34 different 2D materials studied. Moreover, based on the knowledge of the method and chemical information of the material, we can predict the small number of cases in which the method is not so effective and also provide the best recipe for an optimized DFT-1/2 method based on the electronegativity difference of the bonding atoms.

DOI: 10.1103/PhysRevB.97.045426

I. INTRODUCTION

The synthesis of isolated graphene from graphite exfoliation in 2004 [1] and its unique properties gave rise to a totally new research field dedicated to the study of novel two-dimensional (2D) materials. In recent years, the scientific community has studied several monolayer materials beyond graphene [2–6], among which are IV-A elements such as silicene [7], germanene [8,9], stanene [10] honeycomb structures made of group III-A and V-A atoms, such as hexagonal boron nitride (hBN) [11], and transition-metal dichalcogenides (TMDCs) [12,13]. The spectrum of electronic properties available within the library of 2D crystals ranges from insulating properties in hBN to semiconducting, metal, and superconducting ones in TMDCs [13,14]. A large variety of electronic properties in 2D elemental group-V materials, binary III-VII and IV-VI compounds, and ternary III-VI-VII and IV-V-VII compounds has been also recently reported [15]. These new classes of materials pave the way not only for understanding new physics, but also for the application of these materials to novel electronic and optoelectronic devices.

Electronic structure is a fundamental property, and its accurate description is the basis for further study of electronic and optical properties. It has been well established that the many-body effects on the electronic structure are greatly enhanced in low-dimensional systems [16]. Within theoretical studies, *ab initio* calculations based on density functional theory (DFT) [17] are often used in the computational prediction of physical properties of novel materials. This approach achieved great success regarding ground state properties, such as total energies, bond lengths, and lattice parameters. However, accuracy limitations must be considered for properties dependent on excited states, such as in calculations of energy band gaps and dielectric functions. It is well known that the standard DFT approach underestimates the energy band gap, and even predicts semimetallic behaviors instead of semiconducting ones for some pathological cases, such as in the case of bulk InAs and InN [18]. Different theoretical approaches have been proposed to overcome these limitations, thus providing more reliable predictions to physical properties that depend on excited states. The *GW* approximation is considered the state-of-the-art and most accurate method. It estimates the electron self-energy from quasiparticle energy calculations in terms of perturbation theory [19]. Hybrid functionals, which combine standard DFT with Hartree-Fock (HF) calculations, are also popular and robust alternatives, although they depend on adjustable parameters to calculate energy band gaps. The hybrid functional calculations demand greater computational efforts than standard DFT ones, leading to limitations on the size of the simulated systems. This problem is exacerbated when *GW* calculations are considered. Moreover, *GW* calculations for 2D materials pose additional convergence challenges due to the analytical behavior of the 2D electronic screening and the need to remove interactions between period images [20–22]. Therefore, the study of low computational cost methods for obtaining an accurate band structure for this new class of materials is of great importance, and could open an avenue for studying more complex systems, such as van der Waals heterostructures [23,24], crystal defects [25,26], and alloys [18,27].

To improve computational efficiency while keeping a good compromise with accuracy, Ferreira, Marques, and Teles developed the LDA-1/2 method for approximate self-energy corrections within the framework of conventional Kohn-Sham DFT [28], which can be used not only with the local density

*ivanguilhonn@gmail.com
†danielskoda@gmail.com
‡mmarques@ita.br
§lkteles@ita.br

approximation (LDA), but also with the generalized gradient approximation (GGA) [29,30], nowadays usually named DFT-1/2. The proposed method is able to predict the energy gap results with precision similar to that of the aforementioned quasiparticle corrections, but with the same computational effort of standard DFT calculations. This formalism is also free of adjusted parameters.

Particularly, the DFT-1/2 method was first applied for several 3D crystals considering only the self-energy of the hole, since in the vast majority of the cases only the self-energy of the electron in the conduction band had any importance [28]. This occurs due to the fact that for the DFT-1/2 self-energy the chemical bonding and the localization of the hole and electronic valence and conduction bands are important. For 3D crystals, the valence band maximum (VBM) is usually made of the p state of the anion, while the conduction band is usually a mixture of many atomic states, including the valence state of the cation. Thus, the self-energy of the cation could be neglected [30]. More recently, it has been shown that for Ge [31] it was also important to consider the conduction self-energy. Moreover, for the challenging calculation of the gaps of oxides, it was important to take into account the composition of the VBM, which may have some character of d or p states of the cation [32]. In the case of 2D materials, differently from most of the bulk semiconductors for which the majority of bonding is formed by sp^3 hybridization, an sp^2 hybridization is present, or a mixture between sp^2 and sp^3, or other hybridizations, presenting a different chemical bonding. Moreover, the system is planar, which means that it is not clear whether a self-energy correction arising from an atomic potential spherically symmetric will work. Therefore a deeper study of how the DFT-1/2 method can be applied to this class of materials is highly desirable.

Despite the fact that the DFT-1/2 method has already been successfully applied to a few two-dimensional (2D) materials [27,31], insights into the DFT-1/2 performance on this class of materials has not been made until now. To address this issue, in this work, we verify the reliability of the DFT-1/2 method to provide good description of 2D materials and perform a direct comparison between its level of accuracy and the ones obtained with GW and hybrid (HSE) calculations. A whole scenario for the application of DFT-1/2 to simulated 2D materials is presented, and cases in which the methodology succeeds or fails are thoroughly discussed.

The paper is organized as follows. The theoretical background of the DFT-1/2 method and computational details of the calculations performed are presented in Sec. II. The results for the 34 considered materials are presented in Sec. III, in which the accuracy comparison between DFT-1/2 and the HSE06 and GW approaches is discussed. A summary of the presented results and main conclusions can found in Sec. IV.

II. METHODOLOGY

A. Theoretical background

The DFT-1/2 methodology is derived in the spirit of Slater-Janak transition-state theory [33–35], solving the problem of its implementation in the case of infinite solid systems, giving a practical scheme for band gap calculations of semiconductors [28,30].

Janak's theorem [34] states that the derivative of the total energy $E(N)$ of a system with N electrons with respect to the occupancy number f_i of an arbitrary state α is given by its respective Kohn-Sham eigenvalue:

$$\frac{\partial E(N)}{\partial f_\alpha} = \varepsilon_\alpha(f_\alpha). \tag{1}$$

Combined with the assumption of the linearity of the eigenvalues with the orbital occupancies [30,35], one may calculate the ionization energy I and electron affinity A of an N-electron system as

$$I = E(N-1) - E(N) = -\varepsilon_v(1/2) \tag{2}$$

and

$$A = E(N) - E(N+1) = -\varepsilon_c(1/2), \tag{3}$$

where $\varepsilon_v(1/2)$ and $\varepsilon_c(1/2)$ represent respectively the eigenenergies associated with the valence band maximum and conduction band minimum.

While the half-occupation scheme provides accurate atomic ionization potentials, it cannot be directly applied to extended crystalline systems. In the DFT-1/2 approach the orbital-dependent self-energy S_α is considered as a quantum mechanical average of a "self-energy potential" $V_S(\vec{r})$,

$$S_\alpha = \int d^3r\, n_\alpha(\vec{r}) V_S(\vec{r}), \tag{4}$$

of a Kohn-Sham state α with $n_\alpha(\vec{r})$ being its correspondent electronic density. The self-energy potential $V_S(\vec{r})$ is approximately given by the difference between the Kohn-Sham potentials for the half-ionized and neutral atoms:

$$V_S(\vec{r}) = -V(-1/2,r) + V(0,r). \tag{5}$$

In crystals the self-energy correction is obtained by subtracting the self-energy potential $V_S(\vec{r})$ from the local part of the atomic pseudopotential or the $-2Z/r$ part of the all-electron potential. To avoid the penetration of the self-energy Coulomb tails into neighboring atom sites, the self-energy potentials are trimmed according to $\tilde{V}_S = \Theta(r)V_S(\vec{r})$ by a cutoff function $\Theta(r)$:

$$\Theta(r) = \begin{cases} \left[1 - \left(\frac{r}{\mathrm{CUT}}\right)^8\right]^3, & r \leqslant \mathrm{CUT}, \\ 0, & r > \mathrm{CUT}. \end{cases} \tag{6}$$

The value of the cutoff parameter CUT is determined in a variational way to make the band gaps extremal without falling back to empirical parameters.

To describe the excitation of an electron from the valence to the conduction band, then it is equivalent to subtracting a half electron from the valence band maximum and adding a half-electron to the conduction band minimum as illustrated in Fig. 1. Therefore the following one-particle Kohn-Sham DFT-1/2 equation must be solved:

$$\left[-\tfrac{1}{2}\nabla^2 + V_{KS}(\vec{r}) - \tilde{V}_{s,v}(\vec{r}) + \tilde{V}_{s,c}(\vec{r})\right]\varphi_i(\vec{r}) = \epsilon_i\varphi_i(\vec{r}), \tag{7}$$

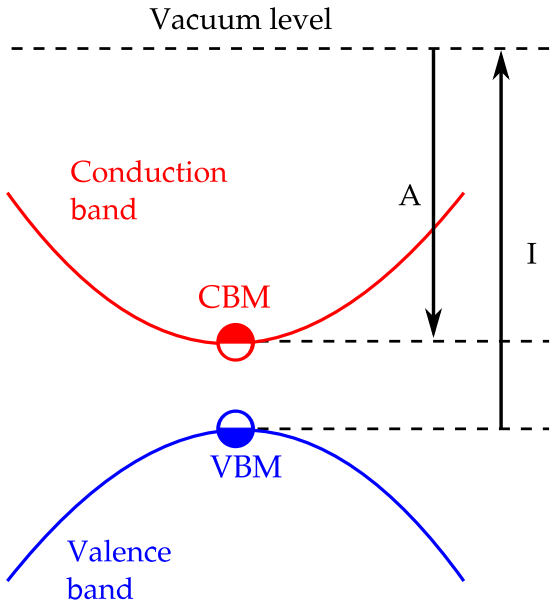

FIG. 1. Half-occupation scheme of DFT-1/2 considering self-energy corrections on valence and conduction bands. A half electron is removed from the VBM, while a half electron is added to the CBM, to corrections on electronic affinity and ionization energy, respectively.

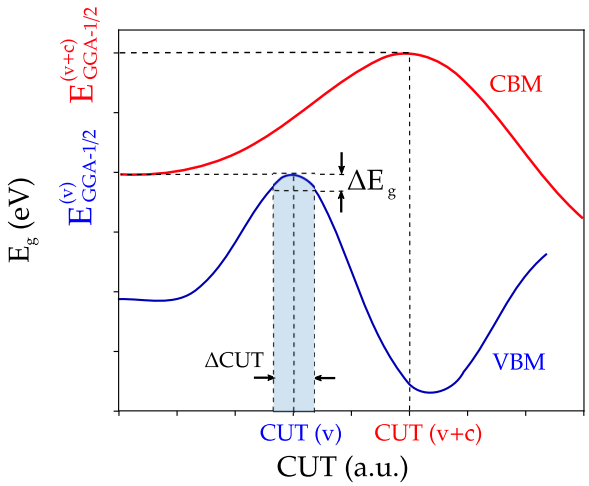

FIG. 2. An example of CUT parameters determination for VBM (CBM) state self-energy potential, represented in blue (red) color. The energy gaps $E^{(v)}_{\mathrm{GGA}-1/2}$ and $E^{(v+c)}_{\mathrm{GGA}-1/2}$ are indicated on the vertical axis. The energy gap sensitivity of ΔE_g due a variation Δ CUT on the cutoff parameter is highlighted for the valence self-energy correction.

where $\tilde{V}_{s,v}$ ($\tilde{V}_{s,c}$) is the trimmed valence (conducting) self-energy potential. Thus the DFT-1/2 energy is directly given by the difference between eigenvalues $\epsilon_c - \epsilon_v$.

In the case of 3D crystals, with the exception of Ge [31], Sn [36], and very ionic compounds [37], only $\tilde{V}_{s,v}$ is considered, as already mentioned.

To apply the DFT-1/2 technique, it is essential to understand the chemistry that lies within the band structure of compounds. Thus, we first investigate the formation of band structures through standard DFT calculations and later employ the DFT-1/2 method. In the case in which the valence (conduction) band has contributions from different atomic orbitals we must remove (add) a smaller fraction of electron from each of them, proportionally to their contribution given by

$$\xi_{x\phi} = \mathrm{char}_{x\phi}[\varphi_\alpha(\vec{k})] \times 1/2, \tag{8}$$

where $\mathrm{char}_{x\phi}[\varphi_\alpha(\vec{k})]$ corresponds to the proportion of the atomic orbital ϕ of the atom x to the orbital character of the Kohn-Sham state φ_α at point $\vec{k}$, given by the projection of $\varphi_\alpha(\vec{k})$ onto the atomic orbitals.

Considering the fact that sometimes there are very small contributions (below 10%) that can be neglected, it is important to normalize the orbital characters of the considered atoms with respect to their sum, arriving at a set of normalized orbital contributions $\xi'_{x\phi}$ that satisfy

$$\sum_{x\phi} \xi'_{x\phi} = 1/2. \tag{9}$$

Finally, the workflow of the DFT-1/2 is described as follows. A standard DFT (LDA or GGA) calculation is performed and the atomic orbital characters of the VBM and conduction band minimum (CBM) are determined. The first self-energy correction is applied to the VBM states (for the vast majority of 3D crystals we usually stop at this point). Then, when necessary, as for 2D materials as we will see, the self-energy correction for the CBM states is also calculated. In these cases, the electronic structure obtained with valence self-energy correction is used as the starting point for the conduction self-energy correction, as depicted in Fig. 2. The energy band gap calculated considering valence and valence+conduction self-energy corrections are denoted as $E^{(v)}_{GGA-1/2}$ and $E^{(v+c)}_{GGA-1/2}$, respectively.

Since the valence and conduction cutoff parameters CUT(v) and CUT(c) are determined by a maximization of $E^{(v)}_{GGA-1/2}$ and $E^{(v+c)}_{GGA-1/2}$ gaps, the energy gap sensitivity ΔE_g for small Δ CUT variations is typically low (see Fig. 2). For this reason, the determined pseudopotential file for the same element can be often transferred from one material to another.

In the simplest case the VBM and CBM states have strong orbital contributions from a single atomic orbital from distinct atoms; in this case a half electron is removed (added) at once and the atomic self-energy is expected to have its best performance. One may verify that the self-energy potential $\tilde{V}_{s,v}$ ($\tilde{V}_{s,c}$) added in Eq. (7) results in stronger corrections on eigenvalues associated with the $\varphi_\alpha(\vec{k})$ states with stronger contributions of the atomic orbital of the VBM (CBM) due to different localization of electronic density of the Kohn-Sham states. Therefore, in this ideal case $\tilde{V}_{s,v}$ corrects the VBM states while $\tilde{V}_{s,c}$ corrects the CBM states.

At this point we already see a limitation of the method. Sometimes, when the VBM and CBM are formed by the same atomic orbitals from the same atom, the self-energy potential corrections on the ϵ_v and ϵ_c eigenvalues are indistinct. This is due to the hypothesis of the quantum mechanical average and the spherical symmetry approximation of the self-energy potential expressed in Eq. (5). In this context, the correction will increase or decrease both levels at the same time, thus keeping the energy gap unaffected.

As a benchmark for the DFT-1/2 performance on the band gap calculation, we consider hybrid functionals

(HSE06) and *GW* quasiparticle corrections, as explained bellow.

The Hartree-Fock method leads to exact exchange energies [38], although it does not consider any correlation interaction between the calculated orbitals constituting the Slater determinant. In order to improve the description of the exchange-correlation interaction, the DFT and HF approaches can be combined into hybrid functionals, in which the exchange energy is taken as a weighted average of Hartree-Fock and standard DFT contributions, while the correlation energy is estimated according to a DFT approximation.

To improve convergence time for big molecules and solids, specially for metallic materials, Heyd, Scuseria, and Ernzerhof proposed a screened Coulomb potential to the exchange interaction in order to screen the long-range part of the HF exchange and spare computational effort [39]. In order to combine good precision with fast convergence, the averaged Hartree-Fock and PBE exchange contributions are only applied to the short-range domain, while long-range exchange interaction only considers the PBE functional. Although providing a faster convergence with respect to standard hybrid approximations, the screened hybrid functional can still increase the computational time costs by two orders of magnitude when compared to the DFT-1/2 approach [18]. This approach is also dependent on adjustable parameters. We consider in this work the HSE06 functional [39–41], which corresponds to a Hartree-Fock weight $\alpha = 0.25$ and the screening value $\mu = 0.2$ Å^{-1}.

More accurate results can be obtained within the combination of many-body perturbation theory with the electronic structure calculated by DFT approach. The quasiparticle energies are solutions of a one-electron equation that considers a self-energy operator $\Sigma(\vec{r},\vec{r'},e_n^{\mathrm{QP}})$ [19]. This last quantity is approximated by the first term of an expansion in Feynman diagrams, which is the product of a Green's function G and the screened Coulomb interaction W. Since G and W depend on the quasiparticles eigenvalues, a solution can be obtained with a self-consistent scheme starting from the DFT wave functions and eigenvalues. However, due to the great amount of computer cost demanded, the W (and G) quantity (quantities) can be estimated with "single-step shots," which is known as the GW_0 (G_0W_0) approximation [42].

It is worth mentioning that for 2D materials with a large energy gap, such as hBN, the choice of performing or not self-consistent calculations of G and W terms may lead to differences up to 1 eV in energy gaps [43]. It has been demonstrated that *GW* calculations of 2D materials exhibit slow convergence, dependent on the vacuum thickness of the simulated supercell, number of the considered unoccupied states, and k-point sampling of the Brillouin zone [22,43]. Therefore, *ab initio* calculations based on quasiparticle *GW* self-energy corrections demand careful convergence studies and may strongly depend on simulation parameters as can be verified comparing different calculations available in the literature, e.g., the discrepancies between the GaN and InN energy gaps calculated by Sahin *et al.* [3] and Prete *et al.* [44]. The computer time demanded by simulations based on the *GW* approximation can be larger than that for DFT-1/2 ones by three orders of magnitude, with a significant memory consumption enhancement [18]. Therefore, the size of feasible systems can be dramatically limited by the availability of computer resources.

B. Computational details

In this work, *ab initio* simulations are calculated as implemented in the Vienna Ab initio Simulation Package (VASP) code [45,46]. Kohn-Sham equations are solved using the projector augmented wave (PAW) scheme [47,48] leading to all-electron wave functions of the valence electrons. Electronic properties are investigated within the DFT by applying the Perdew-Burke-Ernzerhof (PBE) functional within the general gradient approximation (GGA) [49] combined with the previously described DFT-1/2 method. The energy cutoff for the plane-wave expansion was set as 500 eV and a $12 \times 12 \times 1$ Γ-centered Monkhorst-Pack k-point mesh [50] was employed to sample the first Brillouin zone. In order to obtain the equilibrium configurations, structural geometries are optimized using GGA-PBE and all atomic coordinates are relaxed until the Hellmann-Feynman forces are smaller than 1 meV Å^{-1}. Each simulated two-dimensional material is modeled as an artificial 3D periodic crystal constituted by a repetition of atomic layers, separated by a distance of $L = 20$ Å in the out-of-plane direction, which is large enough to render interactions between neighboring sheets negligible. The obtained energy gaps are compared with energy gaps calculated with the hybrid functional HSE06.

III. RESULTS AND DISCUSSION

A. Atomic orbital contributions to VBM and CBM states

A previous DFT calculation for analyzing the chemical bonding and corresponding information of the orbital contributions for the VBM and CBM is the first step for applying the self-energy correction. This information for each of the 2D crystals studied in this work is summarized in Fig. 3. Using the notation from Eq. (8), this diagram supplies us with $\mathrm{char}_{x\phi}$, from which the set of orbital contributions $\xi'_{x\phi}$ can be derived and later employed in the DFT-1/2 method. As discussed earlier, the variation ΔE_g of the energy gap with respect to vanishing contributions from orbitals is small, as their effect on the approximate quasiparticle correction is proportionally less influential than its counterparts. This allows $\xi'_{x\phi}$ to be calculated with approximate orbital composition, provided that $\mathrm{char}_{x\phi} > 10\%$.

For honeycomb materials based on the IV group, valence states are associated with p_z orbitals of the more electronegative element in the binary material, whereas the z direction is adopted as the one perpendicular to the atomic plane. Energy gaps are mostly direct, located at the K point. The only exception is SnC, which has an indirect K-Γ band gap. The CBM states located at the K point can be associated with p_z orbitals of the least electronegative element, while in SnC the CBM state located at the Γ point is derived from a hybridization of s states roughly equally from both carbon and tin atoms.

Direct gaps located at the K point are obtained for materials based on boron, namely BN, BP, BAs, and BSb. These materials exhibit a chemical behavior similar to the one observed for group IV binaries. Their VBM states have strong projections of p_z orbitals of each respective anion, while CBM states are derived from boron p_z atomic orbitals. A different pattern is observed by projecting VBM and CBM states on atomic orbitals for other honeycomb binary materials based on III-V

FIG. 3. Valence and conduction band states projected onto atomic orbitals for the 34 crystals studied. Red, green, and blue colors depict contributions of s, p, and d orbitals to valence and conduction states, while the position of the bar (left or right) indicates the contribution of each atom (cation or anion, respectively) to the formation of the state. The size of the bar is proportional to the relative contribution of each orbital, and their numeric values are indicated for contributions superior to 11%. Upper bars are relative to the conduction band minimum (CBM) and lower bars are relative to the valence band maximum (VBM) within a 2D crystal.

elements. For such materials, a K-Γ indirect band gap is obtained. The VBM states located at the K point are integrally derived from the anion p_z atomic orbitals, while CBM states have a strong s character distributed among both elements. InSb has one singular behavior where the VBM state is derived from p_x and also presents a direct gap, which is now located at the Γ point.

Materials based on Hf and Zr exhibit CBM states based on d states of the transition metals. VBM states are dominated by p orbitals from the chalcogen elements. Pt-based TMDCs exhibit a similar trend, but with a greater mixture between its constituents. PtS_2 and $PtSe_2$ present a VBM made from p orbitals from the chalcogen and p and d orbitals from platinum. Its CBM, on the other hand, is amalgamated by d orbitals from Pt, as well as s and p orbitals from the anions. Quite similar to the tendency of Pt are SnS_2 and $SnSe_2$, whose VBM states originate from a hybridization from s and p states from both constituent elements. CBM states still follow the trend of originating from chalcogen p states.

For all the previously mentioned materials, as also for $HfSe_2$, and $ZrSe_2$, the VBM and CBM exhibit distinct projection on atomic orbitals. Therefore, a good performance of the DFT-1/2 method is expected for these materials.

On the other hand, the majority of the TMDC materials exhibit distinct chemical trends compared to honeycomb materials. Crystals based on Mo and W have VBM and CBM states strongly based on d atomic orbitals. In MX_2 (M = Mo, W; X = S, Se, Te), VBM states are a mixture from in-plane orbitals d_{xy} and d_{x^2} from the cation and p_x and p_y orbitals from the anion. On the other hand, CBM states are largely from out-of-plane d_{z^2} orbitals from the cation, with smaller contributions from s orbitals of the metal and p_x and p_y

orbitals from the anion. As the DFT-1/2 atomic self-energy correction is spherically symmetric, there is no expressive distinction between the self-energy correction of the in- and out-of-plane d orbitals. Therefore, the DFT-1/2 correction will not be effective.

The same occurs for phosphorene, for which the VBM and CBM states are quite similar, made primarily of p orbitals. They differ by a directional reference: while the CBM states are mainly composed by 68% of p_z orbitals and 18% of p_x orbitals (plus 14% by the spherically symmetrical orbitals), 91% of its VBM is made from p_z orbitals. In the latter, only 3% of the contribution to the band state is made by in-plane p_x orbitals.

As previously reported for several 3D materials [30], in the studied materials one may observe that a CUT(v) parameter has a strong dependence on the considered element where the half occupation is applied, which is consistent with the environment neglect and the isolated atom approximation for the self-energy potential. The cutoff parameter and bond lengths are listed in Table I for comparison. The significant differences between CUT parameters for one element in distinct materials is explained by the difference between bond lengths in the studied materials. In general, materials with smaller first-neighbor lengths exhibit smaller cutoff parameters. A linear relation between the CUT parameter and the bond lengths (d) is observed for each class of 2D materials, according to their structures. The relation $\mathrm{CUT(v)} = 0.785 + 0.688d$ is observed for group IV and III-V honeycomb crystals, and in the case of TMDCs, for those with CUT(v) different from zero, the relation $\mathrm{CUT(v)} = 2.919 + 1.283d$ is observed. In particular, $PtTe_2$ and phosphorene are pathological cases. Therefore, in general a trend is seen for each group of 2D crystals. The obtained CUT parameters are illustrated in Fig. 4.

Another important aspect to be analyzed is the transferability of the self-energy potentials. From Fig. 4 one observes that for a given atom and bonding type, the value of CUT depends little on the chemical environment, especially for VBM corrections. Because we are using CUT values that make the gaps extreme, small deviations from the optimal values produce only second-order deviations in the gaps. In our results variations of $\Delta\,\mathrm{CUT} = \pm 0.5$ bohrs on cutoff parameters typically leads to energy gap variations ΔE_g of order a few tenths of eV. Therefore, we conclude that is very reasonable to consider the same CUT(v) value for the anion potentials. X-C (X = Si, Ge, Sn) crystals based on IV-A atoms, for example, have their valence band correction CUT pretty close to each other, ranging from 3.10 to 3.44 bohrs. While they are close to each other, the increase of the bond length also tends to slightly enlarge this parameter. III-V 2D materials also have the same tendency. The CUT value increases for P- and As-based compounds along the family B-Ga-In. 2D nitrides also have their CUT pretty close. Finally, for successful TMDCs, the CUT is clearly linked to the chalcogen atom, presenting almost the same CUT.

The tendencies among the CUT parameter for the correction of the conduction band are similar, although not as clear as the ones observed in the valence band. For tin-based IV-A crystals, these values are quite similar, with deviations smaller than 0.3 bohrs from one to another. IV-A carbides, on the other hand, have an optimal CUT varying from 2.56 to 3.72 bohrs for GeC and SnC, respectively. This seeming lack of relationship between the optimal CUT for the conduction band and the 2D crystal may be related to the varying composition of the CBM for each one of these materials, as depicted in Fig. 3. Since the character of the bands changes along the family of 2D carbides, perfect analogies between the materials are not totally unexpected. Among III-V crystals, boron- and gallium-based ones clearly present the same tendency observed in the VBM correction. The conduction band of BN, however, is an exception, probably due to its smaller lattice parameter. Figure 4 also elucidates the trends for the same anion, showing that phosphides and arsenides present optimal values for the CUT parameter that are quite close. Finally, similarities between the CUT for CBM corrections are clear for the TMDCs under analysis, as well as for SnX_2 (X = S,

TABLE I. DFT-1/2 CUT length for the valence (v) and valence and conduction (c) band corrections, in bohrs. The first-neighbor distances d are listed for comparison with the cutoff parameters and also given in bohrs.

Material	CUT (v)	CUT (c)	d
Group-IV-based honeycomb crystals			
SiC	3.13	2.79	3.38
GeC	3.20	2.56	3.53
SnC	3.44	3.72	3.92
SnGe	4.25	3.61	4.91
SnSi	4.39	3.90	4.84
Groups III-V binary honeycomb crystals			
BN	2.52	1.22	2.74
AlN	3.38	0.00	3.41
GaN	3.12	2.93	3.50
InN	3.17	2.62	3.91
InP	3.86	3.87	4.70
InAs	4.00	3.67	4.92
InSb	4.31	3.50	5.30
GaAs	3.85	3.30	4.55
BP	3.27	3.24	3.51
BAs	3.42	3.37	3.69
GaP	3.68	3.18	4.32
AlSb	4.31	4.61	4.95
BSb	3.84	3.69	4.08
Transition-metal dichalcogenides			
HfS_2	3.37	3.30	4.82
$HfSe_2$	3.56	3.38	5.05
MoS_2	0.00	2.25	4.56
$MoSe_2$	0.00	2.51	4.80
$MoTe_2$	0.00	3.00	5.16
PtS_2	2.84	1.68	4.54
$PtSe_2$	3.17	1.80	4.78
$PtTe_2$	1.17	2.31	5.10
WS_2	0.00	2.37	4.59
WSe_2	0.00	2.51	4.80
WTe_2	0.00	3.50	5.16
ZrS_2	3.37	3.32	4.86
$ZrSe_2$	3.60	3.39	5.09
Group IV dichalcogenides and phosphorene			
SnS_2	3.43	2.90	4.90
$SnSe_2$	3.64	2.93	5.16
Phosphorene	3.16	0.75	4.27

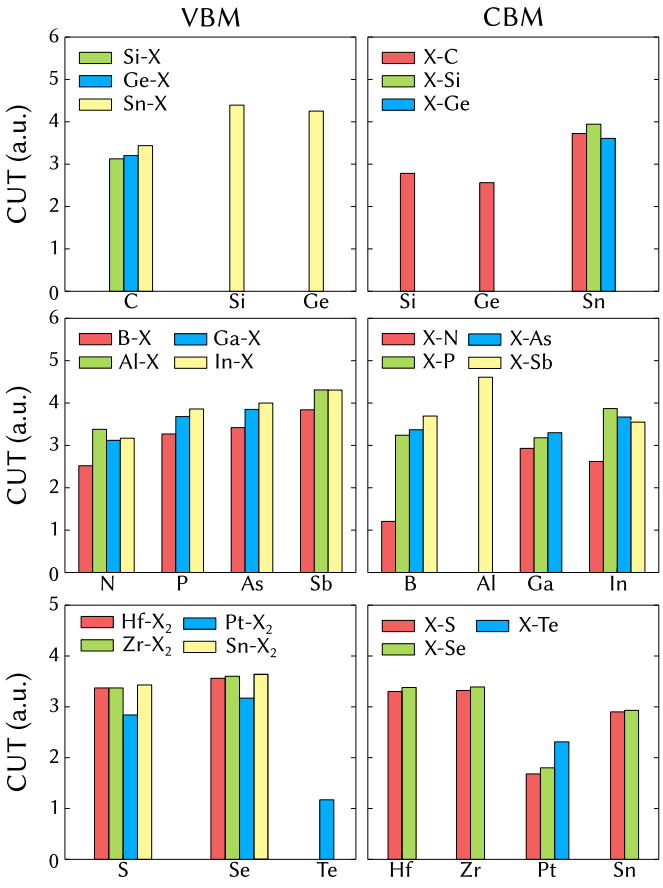

FIG. 4. Cutoff parameter comparison for a selected set of 2D materials. The cutoff parameters of the VBM (CBM) states on the anions (cations) are represented on the left (right).

Se). The CUT parameter deviates by less than 0.1 bohrs when sulfides and selenides are compared. The chemical similarity between Zr and Hf reflects on their close CUT values.

B. Comparison of GGA-PBE, HSE06, GW, and DFT-1/2 band gaps

We performed GGA-PBE, HSE06, and DFT-1/2 calculations for all the 34 considered materials and compared with other available results considering other calculations that consider both hybrid functionals [24,51,52] and different *GW* approximations [3,22,44,53–55]. The obtained results are listed in Table II. The DFT-1/2 method exhibits different performances according to chemical and electronic characteristics from each material. The result trends can be graphically verified in Fig. 5, in which the DFT-1/2 performance is classified in three situations: energy gap results between HSE06 and *GW* results (green area), results that are closer to HSE06 results than GGA-PBE (yellow area), and results that calculated energy gap corrections below 50% of the ones estimated by the HSE06 approach (red area). The areas are mirrored with respect to the 100% standard for a more clear comparison and benchmark. In cases in which DFT-1/2 is overestimated with respect to *GW* approximations, equivalent absolute disagreement tolerances with *GW* results are taken.

TABLE II. Band energy gaps (in eV) for 2D binaries obtained with the DFT-1/2 considering both the corrections only on the valence band (v) and the corrections on valence and conduction bands (v+c), compared with pure GGA, hybrid functionals, and *GW*. In our calculations, we considered GGA-PBE and HSE06 functionals.

Material	GGA	Hybrid	*GW*	DFT-1/2 (v/v+c)
Group-IV-based honeycomb crystals				
SiC	2.54	3.35, 3.46[b]	4.19[a], 4.42[c]	3.90/4.38
GeC	2.10	2.87, 2.85[b]	3.83[a]	3.43/3.87
SnC	0.93	1.78	2.43[g]	1.79/2.07
SnGe	0.23	0.35	0.4[a]	0.63/0.93
SnSi	0.25	0.38	0.68[a]	0.69/1.18
Groups III-V binary honeycomb crystals				
BN	4.65	5.70	6.86[a]	6.62/6.85
AlN	2.91	4.04	5.57[a]	4.87/4.87
GaN	2.16	3.44	4.1[d]	3.64/3.81
InN	0.56	1.53	1.7[d]	1.90/1.98
InP	1.06	1.88	2.88[a]	1.71/2.03
InAs	0.79	1.47	2.07[a]	1.37/1.58
InSb	0.68	1.30	1.84[a]	0.95/1.18
GaAs	1.09	1.91	2.96[a]	1.65/1.99
BP	0.90	1.37	1.81[a]	1.90/3.05
BAs	0.76	1.17	1.24[a]	1.74/2.89
GaP	1.68	2.65	3.80[a]	2.28/2.69
AlSb	1.42	2.02	2.16[a]	1.95/2.26
BSb	0.32	0.61	0.23[a]	1.09/2.16
Transition-metal dichalcogenides				
HfS_2	1.25	2.03[h]	2.98[e]	2.45/2.99
$HfSe_2$	0.54	1.18[h]	1.96[e]	1.65/2.18
MoS_2	1.78	2.25[h]	2.48[e]	1.78/1.91
$MoSe_2$	1.48	1.95[h]	2.18[e]	1.48/1.61
$MoTe_2$	1.18	1.57[h]	1.71[e]	1.18/1.21
PtS_2	1.83	2.64[h]	2.95[e]	2.01/2.06
$PtSe_2$	1.37	1.91[h]	2.48[e]	1.80/1.86
$PtTe_2$	0.46	1.08[h]	1.69[e]	0.63/1.14
WS_2	1.80	2.29[h]	2.43[e]	1.80/1.92
WSe_2	1.62	2.11[h]	2.08[e]	1.62/1.69
WTe_2	1.10	1.52[h]		1.10/1.23
ZrS_2	1.05	1.85[h]	2.88[e]	2.16/2.71
$ZrSe_2$	0.56	1.10[h]	1.85[e]	1.61/2.15
Group IV dichalcogenides and phosphorene				
SnS_2	1.54	2.36[h]	3.07[e]	2.42/2.72
$SnSe_2$	0.74	1.38[h]	1.91[e]	1.53/1.80
Phosphorene	0.79	1.45[i]	2.29[f]	1.39/1.39

[a]Ref. [3] (GW_0).
[b]Ref. [51] (HSE06).
[c]Ref. [53] (*GW*).
[d]Ref. [44] (GW_0).
[e]Ref. [54] (G_0W_0).
[f]Ref. [22] (GW_0).
[g]Ref. [55] (G_0W_0).
[h]Ref. [24] (HSE06).
[i]Ref. [52] (HSE06).

For group-IV-based honeycomb crystals, HSE06 energy gaps are systematically underestimated in comparison with *GW* ones. The considered binary materials present energy gaps which can be related with the electronegativity difference between the constitutive elements in each sublattice. The

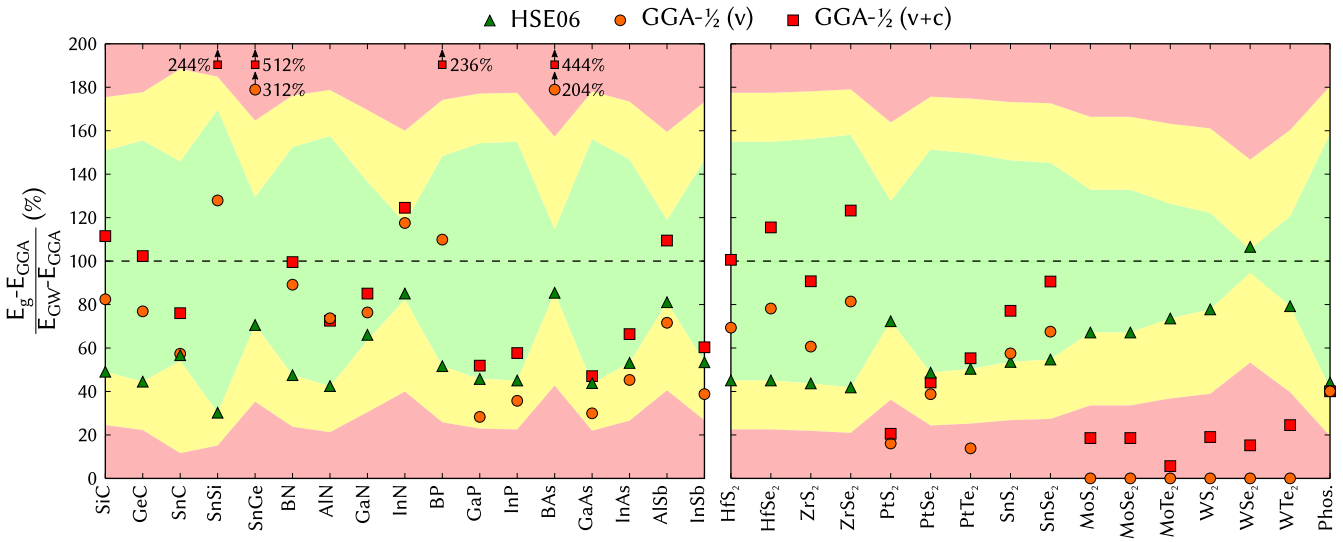

FIG. 5. Comparative performance between GGA-PBE, HSE06, GW_0, and DFT-1/2. DFT-1/2 results considering only VBM self-energy (v) and considering both VBM and CBM (v+c) are depicted with orange circles (red squares), while the HSE06 result is shown with green triangles. The relative energy gap correction is normalized by considering 0% as equal GGA-PBE result and 100% as the *GW* result. The green area is defined by results with calculated band gaps that lie between the HSE06 and *GW* gaps, while the yellow (red) region is defined by results that provide energy gap corrections between 50% and 100% (below 50%) of the energy gap correction obtained by HSE06.

energy gap observed in carbides are, therefore, larger than IV-based honeycomb crystals based on only Si, Ge, and Sn [3,27]. For considered carbides, DFT-1/2 provides energy gaps between HSE06 and *GW* approximation, which are considered as satisfactory results depicted in the Fig. 5 green area. For SnSi and SnGe the self-energy correction is overestimated by about 0.5 eV. This results in very large relative errors in Fig. 5, since the absolute energy gap values are only tenths of an eV. This indicates that the quality of the atomic approximation of the self-energy potential depends on the electronegativity between neighbor atoms.

For most III-V binary honeycomb crystals, the DFT-1/2 method provides energy gaps that fulfill the satisfactory criteria adopted in Fig. 5. For many other III-V binary compounds result comparisons between the different approaches show a strong consistency between them. For III-V materials that do not contain boron, the VBM and CBM projections on atomic orbital fraction are significant on two or even three atomic orbitals. For these materials, the fractional removal of a half electron delivers a DFT-1/2 performance compatible with hybrid functionals. For III-V materials that contain boron, DFT-1/2 delivers a result in excellent agreement with *GW* results for BN, while significantly overestimating the BP, BAs, and BSb energy gaps. These three boron-containing materials exhibit very low electronegativity difference, as previously observed for SnSi and SnGe. This fact suggests that the electronegativity difference between neighbor bonding atoms works as an indicator of the quality of the atomic approximation to the self-energy potential. For these materials, the results considering only the valence band self-energy correction are significantly better, satisfying even satisfactory standard in the cases of SnSi and BP, which is in agreement with the fact that the small electronegativity difference between first-neighbor elements leads to more delocalized conduction states.

For the TMDCs analyzed, Hf-, Sn-, and Zr-based dichalcogenides are materials in which the DFT-1/2 technique is most successful. Its band gaps are comparable to those obtained with GW_0 calculations and always better than those from HSE06 calculations. The deviation from the GW_0 energy gaps obtained in these calculations, when DFT-1/2 is employed, with corrections both in the valence and conduction bands, does not surpasses 25%, as opposed to the deviations larger than 45% from HSE06 results. These crystals have clear chemical tendencies. When observed from the point of view of their characters, these crystals have a conduction band dominated by cation states and valence band generated mostly by anion states. Furthermore, the orbitals composing the bands do not have preferential directions, rendering the *nl* quantum numbers enough to describe the system. In this context, well-localized electrons and holes allow us to apply the DFT-1/2 method exactly in the way it was designed for. The chemical similarities with bulk materials indicate that the success of these materials is related to the anisotropy of 2D systems in the framework of 3D simulations, as well as the chemical composition of the materials. Indeed, the least successful crystals of this group, SnS_2 and $SnSe_2$, present a higher mixture in their conduction band composition than the other TMDCs. Furthermore, these crystals have a higher Pauli electronegativity difference, which supports the hypothesis of a better DFT-1/2 performance for more localized electrons.

The same trend is valid when platinum dichalcogenides are analyzed. While DFT-1/2 grossly underestimates the band gap for PtS_2, $PtSe_2$ and $PtTe_2$ have a better result when both the valence and conduction bands are corrected. In the latter two cases, the band gap is comparable to that obtained from HSE06, but smaller than the GW_0 gaps. The underestimation with respect to this ideal value is about 0.6 eV for $PtSe_2$ and $PtTe_2$, but 0.9 eV for PtS_2.

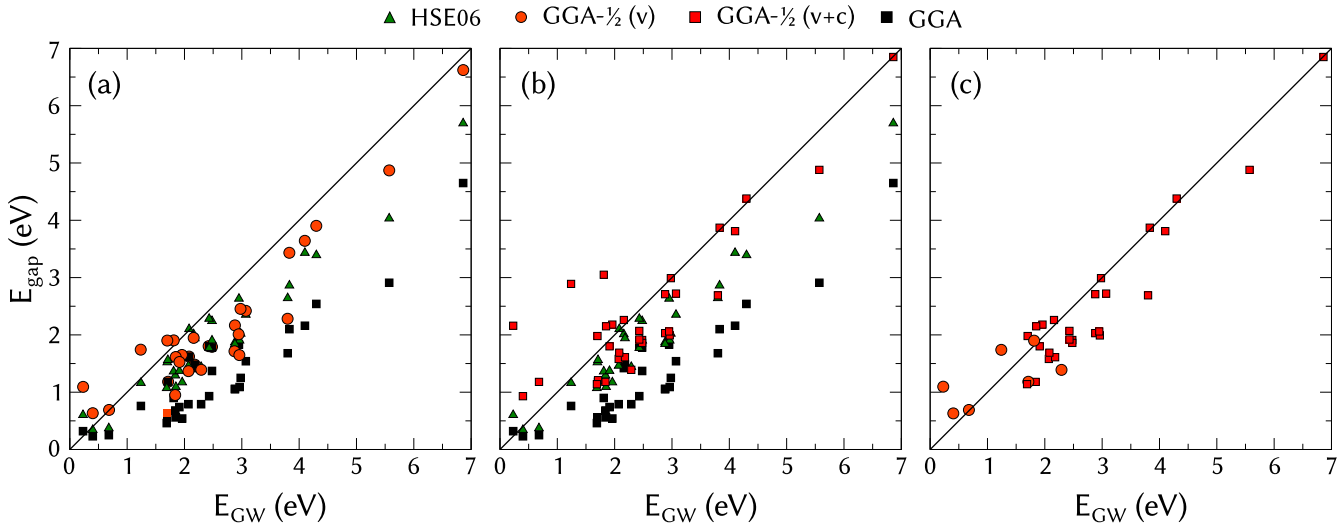

FIG. 6. Comparison of absolute energy band gaps calculated using *GW* and (a) GGA, HSE, and DFT-1/2 (v), (b) GGA, HSE, and DFT-1/2 (v+c), and (c) final DFT-1/2 results, considering the electronegativity threshold of 0.15. The black squares, up-pointing green triangles, orange circles, and red squares represent the GGA, HSE, GGA-1/2 with only valence self-energy correction, and GGA-1/2 with valence and conduction self-energy corrections, respectively. The solid black line illustrates the perfect agreement with the considered *GW* results.

Phosphorene is a crystal which does not have cations and anions. However, its chemical composition, as stated earlier, makes both its valence and conduction bands quite similar. Since the conduction and valence bands are made by p orbitals, the DFT-1/2 correction, as applied to all atoms, is not effective, since both bands are affected together. That way, the addition of a potential relative to the removal of half an electron from the $3p$ shell is not as effective in employing the quasiparticle corrections as in bulk cases, or even in the successful crystals mentioned earlier. Indeed, the band gap obtained with phosphorene is worse than HSE06, but its underestimation does not surpasses 0.1 eV with respect to this method. Both methods fail to describe the larger GW_0 gap for this system, whose band gap is about 0.8 eV greater than those obtained from HSE06 and DFT-1/2.

In the case of crystals such as MX_2 (M = Mo, W; X = S, Se, Te), as previously seen in Sec. III A, the DFT-1/2 method is not effective. A chemical explanation can be derived from the observation of Fig. 3. These materials have their CBM and VBM predominantly made from the cation d orbitals, which hinders the application of the correction proposed by the DFT-1/2 technique. The removal of the electron and later application of the correction potential affects, therefore, the conduction and valence bands by the same quantity. As a consequence, the eigenvalues for these systems merely shift downwards with respect to the vacuum level when a tentative correction is applied to the valence band. Due to the greater percentage of d orbitals in CBM states, the correction for the conduction band in these materials slightly increases the band gap, but in a rather superficial manner. The impossibility of applying the correction with distinction to m quantum numbers is a major obstacle to the application of the DFT-1/2 method in these TMDCs. HSE06, on the other hand, performs quite well for these crystals, with deviations no larger than 0.23 eV with respect to the G_0W_0 results.

C. General trends

Finally, we evaluate what is the expected precision of the DFT-1/2 valence and conduction self-energy corrections compared with the HSE and *GW* approaches. The general trends of the absolute energy gap values calculated within different theoretical frameworks are summarized in Fig. 6. The black squares illustrate the standard GGA energy band gap results, which are significantly underestimated compared to the *GW* ones, as expected. The root-mean-square error (RMSE) of standard GGA energy gaps, compared with *GW* results, is 1.39 eV. The HSE hybrid functional, whose results are depicted as up-pointing green triangles in Fig. 6, calculates energy band gaps in better agreement with the *GW* approach, but still underestimated with a RMSE of 0.70 eV. One may observe that HSE performance is degraded especially for materials with an energy band gap above 3.5 eV. This dependence of hybrid functional performance on the calculated energy band gaps has been also observed for bulk materials and can be addressed, for example, by a nonfixed choice of the α mixing parameter [56].

Figure 6(a) depicts the GGA-1/2 performance compared with GGA, HSE, and *GW* results when only valence self-energy correction is considered. For materials with a large gap ($E_g > 3.5$ eV), the GGA-1/2 method restricted to only valence self-energy correction already delivers better energy gap results than HSE06, while the two methods exhibit similar performances for materials with moderate energy gaps ($E_g <$ 3.5 eV). The RMSE of the GGA-1/2 method considering only valence state self-energy corrections with respect to *GW* results is 0.70 eV.

The effect of the introduction of the conduction self-energy correction is illustrated in Fig. 6(b). For the vast majority of 2D materials, this approach leads to more accurate results. However, for a small set of materials (BP, BAs, BSb, SnSi, and SnGe) the combination of the two self-energy potentials leads

to overestimated results. This can be explained by a larger delocalization of conduction states, which can be associated with small Pauling electronegativity difference between first-neighbor atoms. In these cases, an overestimation of the self-energy correction estimated with the free atom approximation should be expected. To overcome this obstacle, we identify a threshold of 0.15 as the minimum Pauling electronegativity difference between bonding atoms in order to demand the inclusion of conduction self-energy corrections. When the electronegativity difference is lower than the defined threshold (SnGe, SnSi, BP, BAs, BSb, $MoTe_2$, and phosphorene), the conduction self-energy correction is ignored, while for the other 2D materials valence and conduction self-energy corrections must be considered. The final results, obtained by this described prescription, are depicted in Fig. 6(c) and give a RMSE of 0.53 eV with the same computational cost as a standard GGA calculation.

IV. SUMMARY AND CONCLUSIONS

In summary, we performed a thorough investigation of the DFT-1/2 method applied to 34 different 2D crystals. Differently from the 3D compounds, we found that for the majority of 2D materials the inclusion of the conduction self-energy corrections is important. In the case of mixed VBM (CBM) states, the DFT-1/2 correction is applied by removing (adding) a fraction of a half electron from different atomic orbitals according to the VBM (CBM) atomic character. First, atomic geometries for each crystal were optimized using GGA-PBE, and an investigation of the composition of the conduction and valence bands was performed to analyze the inherent chemical trends within the set of crystals under study. Afterwards, a benchmark using GGA, HSE06, and DFT-1/2 was performed for all crystals, and the results compared with *GW* values from the literature. The transferability of the DFT-1/2 self-energy potentials was investigated through the CUT parameter, which is obtained variationally, and can be related to the lattice parameters and bond lengths.

A discussion on the performance of DFT-1/2 for 2D crystals was made. TMDCs based on Hf, Zr, and Sn presented a very good performance, achieving better results than those from HSE06. PtS_2 did not perform as well, but its DFT-1/2 band gap improved with respect to those from standard GGA calculations. $PtSe_2$, $PtTe_2$, and phosphorene had results comparable to the ones obtained from HSE06 calculations. Mo- and W-based TMDCs had improved by an insignificant amount with the application of DFT-1/2 technique. For group-IV, DFT-1/2 provide energy gaps between the HSE06 and *GW* calculations for the carbides. For the considered III-V materials, the DFT-1/2 approach obtains energy gaps equivalent to the hybrid functional for most of the considered materials, while overestimating the small band gaps of SnSi and SnGe. The same occurs with BP, BAs, and BSb. This behavior was associated with the small electronegativity difference between the bonding atoms, leading to a more delocalized conduction band and an overestimation of the conduction DFT-1/2 self-energy. Thus, we defined a threshold for the Pauling electronegativity difference of 0.15 for inclusion of the conduction self-energy corrections. This results in a very nice agreement between the DFT-1/2 and *GW* results. The overall picture shows that the DFT-1/2 approach calculates energy gaps with RMSE lower than the HSE06 hybrid functional for the considered 2D materials, when compared to the *GW* results, with a small fraction of computer resources necessary of the latter approach. The failures of the method are traced back to the composition of each band based on its orbitals, with the least successful crystals presenting both the CBM and VBM made by the same orbitals and in similar proportions. The absence of 3D symmetry in these systems also renders it impossible to describe well the correction in the self-potential without the m quantum number.

We hope that this work gives grounds for efficient and systematic investigations on 2D physics by using efficient alternatives to quasiparticle corrections within the DFT such as DFT-1/2. Furthermore, the methodology derived here for 2D materials can provide a new perspective for more complex future calculations, such as the inclusion of excitonic effects, including the spin-orbit interaction (a fundamental effect for materials having heavy elements and for topological insulators), to obtain results that can be directly comparable with the experiments, thus expanding the theoretical research on 2D materials.

ACKNOWLEDGMENTS

This work was funded by the Brazilian agencies Fundação de Amparo à Pesquisa do Estado de São Paulo (Grant No. 2012/50738-3), Conselho Nacional de Desenvolvimento Científico e Tecnológico (Grants No. 305405/2014-4 and No. 308742/2016-8), and Coordenação de Aperfeiçoamento de Pessoal de Nível Superior (Programa Professor Visitante do Exterior, Grants No. 88881.068355/2014-01 and No. 88887.116535/2016-00) within the program Science Without Borders.

[1] K. S. Novoselov *et al.*, Science **306**, 666 (2004).
[2] P. Miro, M. Audiffred, and T. Heine, Chem. Soc. Rev. **43**, 6537 (2014).
[3] H. Sahin, S. Cahangirov, M. Topsakal, E. Bekaroglu, E. Akturk, R. T. Senger, and S. Ciraci, Phys. Rev. B **80**, 155453 (2009).
[4] T. Suzuki, Appl. Phys. Lett. **107**, 213105 (2015).
[5] T. Suzuki and Y. Yokomizo, Physica E (Amsterdam, Neth.) **42**, 2820 (2010).
[6] A. L. Ivanovskii, Russ. Chem. Rev. **81**, 571 (2012).
[7] M. Houssa, Appl. Phys. Lett. **97**, 112106 (2010).
[8] M. Houssa, Appl. Phys. Lett. **96**, 082111 (2010).
[9] H. Behera and G. Mukhopadhyay, AIP Conf. Proc. **1349**, 823 (2010).
[10] F. Matusalem, F. Bechstedt, M. Marques, and L. K. Teles, Phys. Rev. B **94**, 241403 (2016).
[11] D. Pacilé, J. C. Meyer, Ç. Ö Girit, and A. Zettl, Appl. Phys. Lett. **92**, 133107 (2008).
[12] S. Z. Butler, S. M. Hollen, L. Cao, Y. Cui, J. A. Gupta, H. R. Gutiérrez, T. F. Heinz, S. S. Hong, J. Huang, A. F. Ismach, E. Johnston-Halperin, M. Kuno, V. V. Plashnitsa, R. D. Robinson,

R. S. Ruoff, S. Salahuddin, J. Shan, L. Shi, M. G. Spencer, M. Terrones, W. Windl, and J. E. Goldberger, ACS Nano **7**, 2898 (2013).
[13] M. Xu, T. Liang, M. Shi, and H. Chen, Chem. Rev. **113**, 3766 (2013).
[14] M. Chhowalla, H. S. Shin, G. Eda, L.-J. Li, K. P. Loh, and H. Zhang, Nat. Chem. **5**, 263 (2013).
[15] Z. Zhu, B. Dong, T. Yang, and Z.-D. Zhang, arXiv:1708.04766.
[16] G. Luo, X. Qian, H. Liu, R. Qin, J. Zhou, L. Li, Z. Gao, E. Wang, W.-N. Mei, J. Lu *et al.*, Phys. Rev. B **84**, 075439 (2011).
[17] W. Kohn and L. J. Sham, Phys. Rev. **140**, A1133 (1965).
[18] R. R. Pela, M. Marques, and L. K. Teles, J. Phys.: Condens. Matter **27**, 505502 (2015).
[19] L. Hedin, Phys. Rev. **139**, A796 (1965).
[20] W. Gao, W. Xia, X. Gao, and P. Zhang, Sci. Rep. **6**, 36849 (2016).
[21] S. Ismail-Beigi, Phys. Rev. B **73**, 233103 (2006).
[22] F. A. Rasmussen, P. S. Schmidt, K. T. Winther, and K. S. Thygesen, Phys. Rev. B **94**, 155406 (2016).
[23] A. Geim and I. Grigorieva, Nature (London) **499**, 419 (2013).
[24] D. S. Koda, F. Bechstedt, M. Marques, and L. K. Teles, J. Phys. Chem. C **120**, 10895 (2016).
[25] F. Matusalem, M. Ribeiro, Jr., M. Marques, R. R. Pelá, L. G. Ferreira, and L. K. Teles, Phys. Rev. B **88**, 224102 (2013).
[26] B. Lucatto, L. V. C. Assali, R. R. Pela, M. Marques, and L. K. Teles, Phys. Rev. B **96**, 075145 (2017).
[27] I. Guilhon, L. K. Teles, M. Marques, R. R. Pela, and F. Bechstedt, Phys. Rev. B **92**, 075435 (2015).
[28] L. G. Ferreira, M. Marques, and L. K. Teles, Phys. Rev. B **78**, 125116 (2008).
[29] R. R. Pelá, M. Marques, L. G. Ferreira, J. Furthmüller, and L. K. Teles, Appl. Phys. Lett. **100**, 202408 (2012).
[30] L. G. Ferreira, M. Marques, and L. K. Teles, AIP Adv. **1**, 032119 (2011).
[31] F. Matusalem, M. Marques, L. K. Teles, and F. Bechstedt, Phys. Rev. B **92**, 045436 (2015).
[32] C. A. Ataide, R. R. Pelá, M. Marques, L. K. Teles, J. Furthmüller, and F. Bechstedt, Phys. Rev. B **95**, 045126 (2017).
[33] J. C. Slater and K. H. Johnson, Phys. Rev. B **5**, 844 (1972).
[34] J. F. Janak, Phys. Rev. B **18**, 7165 (1978).
[35] J. R. Leite and L. G. Ferreira, Phys. Rev. A **3**, 1224 (1971).
[36] F. L. Freitas, J. Furthmüller, F. Bechstedt, M. Marques, and L. K. Teles, Appl. Phys. Lett. **108**, 092101 (2016).
[37] F. Matusalem, A. Filippetti, G. Cappellini, M. Marques, and L. K. Teles (unpublished).
[38] F. Bechstedt, *Many-Body Approach to Electronic Excitations: Concepts and Applications* (Springer-Verlag, Berlin, Heidelberg, 2015).
[39] J. Heyd, G. E. Scuseria, and M. Ernzerhof, J. Chem. Phys. **118**, 8207 (2003).
[40] J. Paier, M. Marsman, K. Hummer, G. Kresse, I. C. Gerber, and J. G. Ángyán, J. Chem. Phys. **124**, 154709 (2006).
[41] J. Paier, M. Marsman, K. Hummer, G. Kresse, I. Gerber, and J. Ángyán, J. Chem. Phys. **125**, 249901 (2006).
[42] M. Shishkin and G. Kresse, Phys. Rev. B **75**, 235102 (2007).
[43] N. Berseneva, A. Gulans, A. V. Krasheninnikov, and R. M. Nieminen, Phys. Rev. B **87**, 035404 (2013).
[44] M. S. Prete, A. M. Conte, P. Gori, F. Bechstedt, and O. Pulci, Appl. Phys. Lett. **110**, 012103 (2017).
[45] G. Kresse and J. Furthmüller, Phys. Rev. B **54**, 11169 (1996).
[46] G. Kresse and J. Furthmüller, Comput. Mater. Sci. **6**, 15 (1996).
[47] P. E. Blöchl, Phys. Rev. B **50**, 17953 (1994).
[48] G. Kresse and D. Joubert, Phys. Rev. B **59**, 1758 (1999).
[49] J. P. Perdew, M. Ernzerhof, and K. Burke, J. Chem. Phys. **105**, 9982 (1996).
[50] H. J. Monkhorst and J. D. Pack, Phys. Rev. B **13**, 5188 (1976).
[51] Y. Rao, S. Yu, and X.-M. Duan, Phys. Chem. Chem. Phys. **19**, 17250 (2017).
[52] D. S. Koda, F. Bechstedt, M. Marques, and L. Kühl Teles, J. Phys. Chem. C **121**, 3862 (2017).
[53] H. C. Hsueh, G. Y. Guo, and S. G. Louie, Phys. Rev. B **84**, 085404 (2011).
[54] F. A. Rasmussen and K. S. Thygesen, J. Phys. Chem. C **119**, 13169 (2015).
[55] T.-Y. Lu, X.-X. Liao, H.-Q. Wang, and J.-C. Zheng, J. Mater. Chem. **22**, 10062 (2012).
[56] M. A. L. Marques, J. Vidal, M. J. T. Oliveira, L. Reining, and S. Botti, Phys. Rev. B **83**, 035119 (2011).